Combination Doppler backscattering/cross-polarization scattering diagnostic for the C-2W field-reversed configuration

L. Schmitz,[1,2,a)] B. Deng,[2] M. Thompson,[2] H. Gota,[2] C. Lau,[2] D. P. Fulton,[2] Z. Lin,[3] T. Tajima,[2,3] M. Binderbauer,[2] and TAE Team[2,b)]
[1]*Department of Physics and Astronomy, University of California Los Angeles, Los Angeles, California 90095, USA*
[2]*TAE Technologies, Inc., Foothill Ranch, California 92610, USA*
[3]*Department of Physics and Astronomy, University of California Irvine, Irvine, California 92697, USA*

(Presented 18 April 2018; received 7 May 2018; accepted 20 June 2018; published online 5 October 2018)

A versatile combination Doppler backscattering and Cross-Polarization Scattering (CPS) diagnostic for the C-2W beam-driven field-reversed configuration is described. This system is capable of measuring density fluctuations and perpendicular magnetic field fluctuations across a wide wavenumber range ($2.5 \le k_\theta \rho_s \le 50$), with typical resolution $\Delta k_\theta / k_\theta \le 0.4$-$0.8$. Four tunable frequencies ($26\ \text{GHz} \le f \le 60\ \text{GHz}$ corresponding to plasma cut-off densities $0.8 \times 10^{19} \le n_e \le 4.4 \times 10^{19}\ \text{m}^{-3}$) are launched via quasi-optical beam combiners/polarizers and an adjustable parabolic focusing mirror selecting the beam incidence angle. GENRAY ray tracing shows that the incident O-mode and backscattered CPS X-mode beam trajectories for C-2W plasma parameters nearly overlap, allowing simultaneous detection of $\tilde{n}$ and $\tilde{B}_r$ or $\tilde{B}_\theta$ from essentially the same scattering volume. *Published by AIP Publishing.* https://doi.org/10.1063/1.5038914

I. INTRODUCTION

Field-reversed configurations (FRCs) are axisymmetric, compact plasmas characterized by high β (the ratio of kinetic to magnetic pressure). Typically, in fusion plasmas, radial particle and heat transport in excess of classical or neoclassical transport is observed, which is caused by plasma turbulence. In the C-2U FRC device at TAE Technologies,[1,2] Doppler Backscattering (DBS) measurements[3,4] with a diagnostic described earlier[5] clearly show that fluctuations at low toroidal wavenumber are absent/stable in the FRC core.[6] Gyrokinetic stability analysis has attributed core stability to the combined effect of large ion Larmor radius, short field-line connection length restricting the parallel wavenumber spectrum, and favorable magnetic field gradient.[7,8] Only low-level electron-scale fluctuations are observed in the FRC core. However, substantial density fluctuation amplitudes with an exponentially decreasing wavenumber spectrum were measured in the scrape-off layer (SOL) and near the excluded-flux radius (near the magnetic separatrix). Anomalous electron radial heat loss is also observed, and the diagnosis of radial magnetic field fluctuations is therefore clearly important. In FRC plasmas, the radial thermal electron heat flux $Q_e{}^t$ is typically anomalously high compared to the classical value. $Q_e{}^t$ can formally be linked to the radial fluxes produced by correlated density, electron temperature, and toroidal electric field fluctuations, and fluctuations of the parallel heat flux and radial magnetic field,[9]

$$Q_e^t = \frac{3}{2}(nT_e)/B\left(\left\langle\left(\tilde{T}_e/T_e\right)\tilde{E}_\theta\right\rangle + \left\langle(\tilde{n}/n)\tilde{E}_\theta\right\rangle\right) + \left\langle\tilde{q}_\parallel\tilde{B}_r\right\rangle. \quad (1)$$

Here, the first two terms on the right-hand side correspond to the electrostatically driven electron heat flux, and the third term describes the electromagnetic contribution.

In an FRC, electromagnetic contributions could be important as β is near unity and well in excess of $(m_e/m_i)^{1/2}$.[10] In this paper, we describe an extension of the existing DBS diagnostic for density fluctuation, capable of measuring in addition spectrally resolved radial or poloidal magnetic field fluctuations via Cross-Polarization Scattering (CPS),[11–17] simultaneously with DBS density fluctuation measurements.

The diagnostic principle of CPS is based on scattering of an incident microwave beam into the opposite polarization. Using the wave equation[15] for the scattered field E_s and the perturbed nonlinear equation of motion for the plasma electrons, the current $J^{(i)}$ induced by the incident wave (with incident electric field E_i) is described by

$$-\nabla\times(\nabla\times\boldsymbol{E}_s) + \left(\frac{\omega_i}{c}\right)^2\left(1 - \frac{\sigma}{i\varepsilon_0\omega_i}\right)\boldsymbol{E}_s = -i\mu_0\frac{\partial\boldsymbol{J}^{(i)}}{\partial t}, \quad (2)$$

$$\boldsymbol{J}^{(i)} = \frac{i\varepsilon_0\omega_{pe}^2}{\omega_i}\frac{\tilde{n}}{n}\boldsymbol{E}_i + \frac{\omega_i}{\varepsilon_0\omega_{pe}^2}\sigma\left[\sigma\boldsymbol{E}_i\times\tilde{\boldsymbol{B}}/B\right]. \quad (3)$$

Here, σ is the unperturbed plasma conductivity. The second term in Eq. (3) describes the electron current induced via cross-polarization scattering. If a Gaussian microwave beam, for example, in O-mode polarization, is launched toward the plasma at an oblique angle to the magnetic flux surfaces, the beam is refracted in the FRC plasma and its trajectory/wavenumber will be approximately toroidal near the

Note: Paper published as part of the Proceedings of the 22nd Topical Conference on High-Temperature Plasma Diagnostics, San Diego, California, April 2018.
a)Author to whom correspondence should be addressed: lschmitz@ucla.edu
b)TAE Team members are listed in Nucl. Fusion **57**, 116021 (2017).

cut-off layer. In addition to backscattering (exploited for density fluctuation measurements via DBS), a fraction of the incident radiation scatters into the opposite (X-mode) polarization. In principle, backscattering and CPS occur along the entire beam trajectory; however, several effects localize the backscattering and CPS response to the cut-off layer, including the reduction of the incident radial wavenumber as the beam approaches cutoff.[3–5] In C-2U and with the expected early C-2W plasma parameters, the calculated O-mode and X-mode cut-off locations are relatively close together, as demonstrated in Fig. 1(a). This is due to the fact that the plasma frequency, ω_{pe}, is substantially above the electron cyclotron frequency ω_{ce} across the FRC core plasma and most of the SOL.

In this paper, we describe a combination DBS/CPS diagnostic planned for the C-2W FRC, which has recently completed construction at TAE Technologies, Inc. The paper is organized as follows: in Sec. II, calculations of the cut-off layer radii for X-mode and O-mode incident polarization are shown. GENRAY ray tracing calculations have been carried out, showing the trajectories of incident and back-scattered microwave beams for different representative expected plasma parameters in C-2W. The beam optics setup and microwave signal detection and processing are discussed in Sec. III. In Sec. IV, limiting geometry considerations and the requirements for beam alignment are discussed.

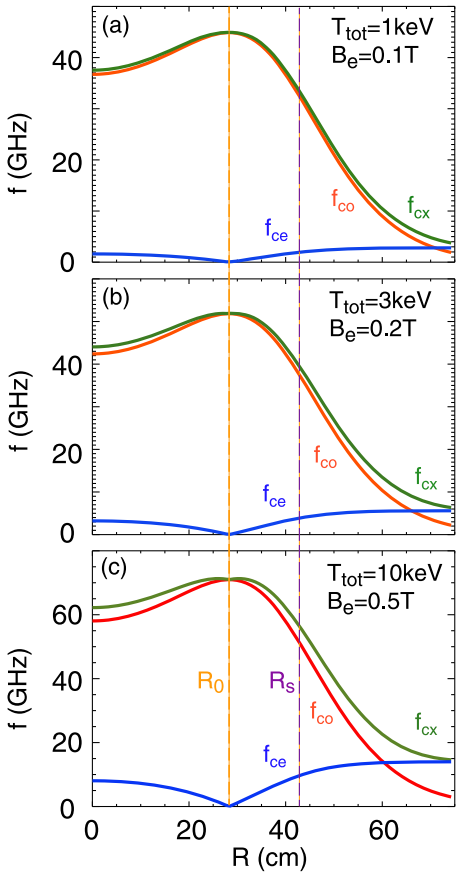

FIG. 1. (a) Cut-off frequency for the X-mode (f_{cx}) and O-mode (f_{co}) vs. radius R, for the initial plasma parameters in C-2W, (b) for expected advanced plasma parameters, and (c) for expected plasma parameters in a future higher–field FRC. The electron cyclotron frequency f_{ce} is also shown. The calculations are based on rigid-rotor equilibria.[18]

II. GENRAY RAY TRACING RESULTS FOR DBS AND CPS BEAM TRAJECTORIES

A thorough understanding of the trajectories of incident and scattered microwave beams, including the cross-polarized feature, is required to evaluate the probed wavenumber and the radial/toroidal location of the cut-off layer. For the initial plasma parameters in C-2W [with external field $B_e \sim 0.1$ T and total (electron + ion) temperature $T_{tot} = T_e + T_i \leq 1$ keV], the X-mode and O-mode cutoff radii are located very closely together, as shown in Fig. 1(a). A rigid-rotor equilibrium,[18] with external field $B_e = 0.1$ T and total temperature $T_{tot} = T_e + T_i = 1$ keV, was used to calculate the cut-off radii. The X-mode and O-mode cutoff locations track very closely in the FRC core, as shown in Fig. 1(a). As C-2W reaches its maximum expected ion energy and external magnetic field [Fig. 1(b)], the X-mode and O-mode cut-off radii separate, in particular in the SOL outside the separatrix ($R \geq R_s$). The effects of a further projected performance increase for a follow-up experiment are indicated in Fig. 1(c). Here, the X- and O-mode cut-off radii are separated considerably in the SOL and in the FRC core plasma. It will be shown in the following Fig. 2, for launched O-mode and initial C-2W parameters, that the cross-polarized X-mode emission can be detected with only minor re-alignment of the (dedicated) receiving X-mode horn antennas, within a few cm off the optical axis. Beam trajectories are calculated with the GENRAY beam tracing code,[19] using the cold plasma dispersion relation, which is adequate for electron temperatures below ~4 keV, well above the projected C-2W electron temperature. Figure 2 shows the results of ray tracing calculations for launched O-mode radiation at different frequencies and toroidal launch angles ζ. The O-mode beam (shown in red) is launched here for simplicity in the C-2W midplane. Within the available launch frequency range of 26-60 GHz, the SOL and the FRC core plasma between the separatrix and the field-null region can be accessed up to a density maximum of 4.4×10^{19} m^{-3}. The O-mode radiation backscattered from the O-mode cut-off layer is detected via monostatic beam optics for DBS (the launch antenna is also used as a receive antenna, and directional couplers are used to separate out the backscatter return). Cross-polarized radiation emission is expected to be most prominent near the X-mode cut-off layer, which is just outside the O-mode cutoff. We focus on backscattering because it allows using monostatic detection for DBS for a large range of toroidal launch angles, providing the toroidal turbulence wavenumber spectrum. The corresponding outbound CPS X-mode ray paths are shown in green and follow a slightly different trajectory than the incoming O-mode due to the higher X-mode refractive index. Dedicated X-mode receive antennas are used that can be independently positioned off-center with respect to the O-mode optical axis via adjustable xyz stages. Ray tracing for a range of toroidal launch angles demonstrates that the maximum expected deviation of backscattered X-mode radiation from the optical axis is <5 cm at the detection location. The probed turbulence wavenumber is predominantly toroidal

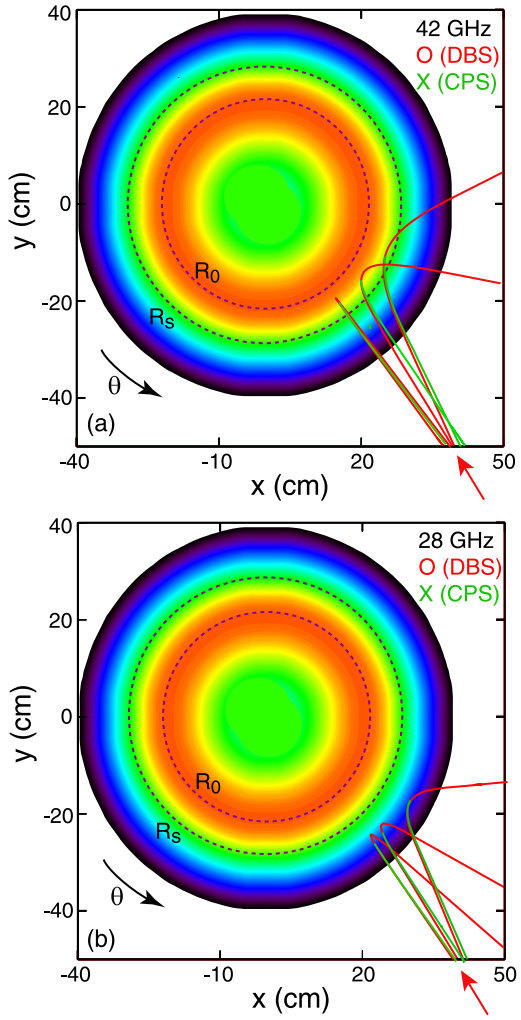

FIG. 2. (a) Ray tracing for launched O-mode (42 GHz, toroidal launch angles with respect to the flux surface normal $\zeta = 0.5°, 5°, 14°$, in red) and backscattered cross-polarization X-mode emission (launched at X-mode cutoff, in green); (b) ray tracing for launched O-mode (28 GHz, $\zeta = 2.5°$, 5°, and 14°, in red) and cross-polarized X-mode, in green; the probed toroidal turbulence wavenumbers are $k_\theta = 0.57$ cm^{-1}, 4.3 cm^{-1}, and 10.2 cm^{-1} for case (a), and $k_\theta = 1.1$ cm^{-1}, 2.2 cm^{-1}, and 5.8 cm^{-1} for case (b). The maximum plasma density (at the field-null radius R_0) is 2.2×10^{19} m^{-3}. R_s designates the separatrix radius. The red arrows indicate the beam launch position/direction; the toroidal coordinate θ is also indicated.

inside the separatrix, but fluctuations with mixed toroidal and radial wavenumbers are detected in the SOL, due to the slightly larger separation between O-mode and X-mode cut-off layers. Since magnetic field fluctuations are expected to have both radial and toroidal wavenumber components, this restriction will likely not impact CPS sensitivity very much. The expected toroidal wavenumber range detectable via CPS is $k_\theta \sim 0.5$-10 cm^{-1} (corresponding to $k_\theta \rho_s \sim 2.5$-50 near the FRC separatrix, with a typical ion sound gyroradius $\rho_s \sim 5$ cm). The lower limit is given by the detectable Doppler shift, and the upper limit is due to the scattering geometry and the expected CPS sensitivity limit, based on previous DBS results for toroidally propagating density fluctuations.[5,6] Simultaneous cross-correlation measurements of density and magnetic field fluctuations in corresponding wavenumber intervals are therefore possible for the first time in FRC geometry. Due to the intrinsic toroidal plasma curvature, the wavenumber response of both DBS and CPS is broadened, as described in Ref. 20 and Sec. IV.

III. BEAM OPTICS AND SIGNAL PROCESSING

A schematic of the measurement principle is shown in Fig. 3. The DBS/CPS diagnostic in C-2W will be located near the axial machine midplane, at a distance of 47 cm from the midplane of the confinement vessel. A total of four channels are implemented (two tunable frequencies in the 26-40 GHz Ka-band and two tunable frequencies in the 40-60 GHz U-band). For each combined (two frequency) channel pair, a Gaussian O-mode microwave beam is launched quasi-optically via a conical scalar horn antenna and an aspherical HDPE (High Density Polyethylene) lens. A beam combiner is used to merge the two frequency bands. The O-mode beam is refracted toroidally near the cut-off location. For DBS, the backscattered O-mode radiation is collected via the same lens/horn combination (monostatic detection, as shown in Fig. 3 for one frequency band). The X-mode signal induced via cross-polarization scattering predominantly originates near the cutoff, where the matching toroidal wavenumber is minimal, according to the Bragg condition (wave momentum conservation). Figure 4 shows the layout of the optical table for the DBS/CPS beam optics. Two scalar horns are used to launch the combined Ka-band and U-band probing beams. An adjustable stainless steel parabolic focusing mirror inside an evacuated enclosure is used to focus the combined probing beams and select the toroidal launch angle ζ. Two-axis adjustability can in addition compensate for axial FRC contraction and the resulting axial misalignment, as discussed in Sec. IV. Two polarizers (copper filaments on a polyester substrate) are used to separate

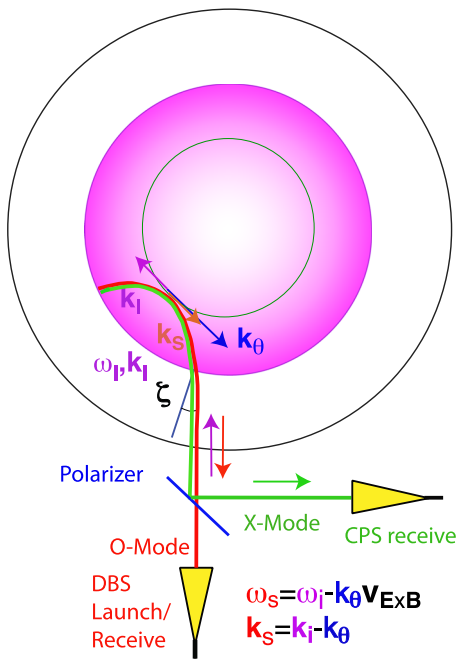

FIG. 3. Schematic of the combination DBS/CPS system, illustrating O-mode launch, ray trajectory in the plasma, O-mode backscattering return (monostatic detection), and X-mode cross-polarization return (CPS receive). The (adjustable) toroidal launch angle ζ with respect to the flux surface normal is indicated.

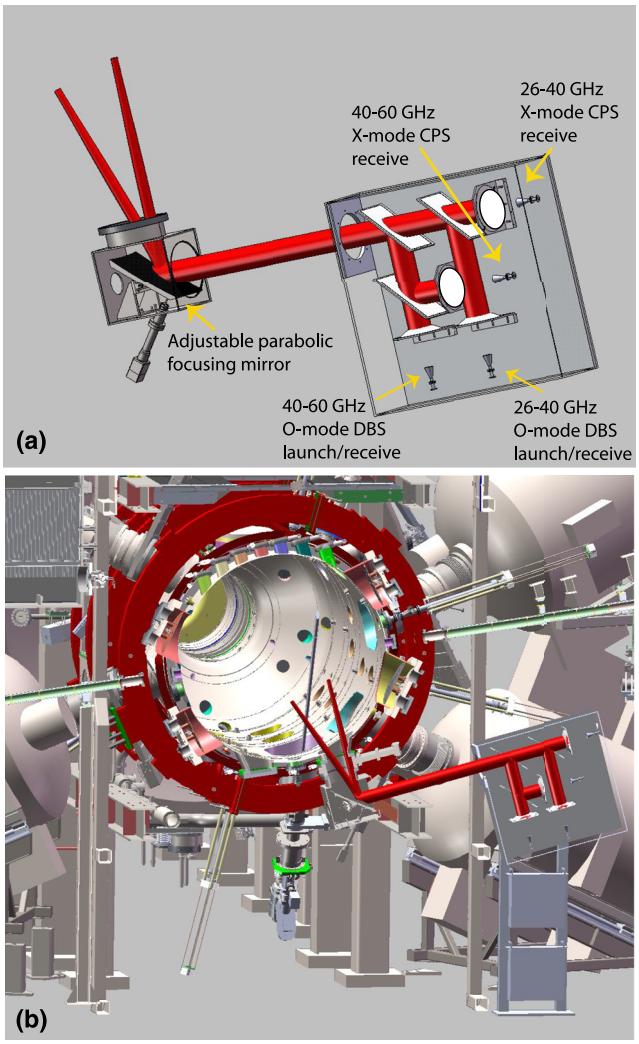

FIG. 4. (a) Layout of the optical board for DBS/CPS beam optics; scalar microwave horns with HDPE lenses, and polarizers are used to launch/receive Ka band (26-60 GHz, two channels) and U-band (40-60 GHz, two channels) for monostatic detection of DBS returns. Separate lensed scalar horns are used to detect the Ka-band and U-band CPS return; (b) diagnostic layout on C-2W.

out the backscattered X-mode cross-polarization signals from the DBS O-mode backscattering return signals. One additional lensed scalar Ka-band horn antenna and one scalar U-band horn antenna are provided to detect the cross-polarization signals.

Figure 5 shows a schematic of the heterodyne microwave transceivers and signal processing electronics for the U-band DBS/CPS system (a similar system will be implemented for the Ka band). The output of two tunable hyper-abrupt varactor-tuned 10-15 GHz oscillators (HTOs) is quadrupled via active frequency multipliers to generate the launched 40-60 GHz probing signals and the difference frequency used for heterodyning. Both channels are combined via a directional coupler to generate the launch signal fed to a scalar U-band horn antenna (typically arranged for O-mode launch). Monostatic detection is used for DBS (the backscattered signal is detected via the same scalar horn and separated out via a directional coupler). Two double-balanced U-band mixers are used to generate intermediate frequency (IF) signals for both channels that are amplified by ~25 dB (amplifiers are not shown here for simplicity) and detected via hybrid in-phase/quadrature (IQ) detectors. The DBS IF section is highlighted in orange in Fig. 5. The local oscillator (LO) input for the IQ detectors is generated via a third double-balanced mixer from the two launched frequencies. The useful frequency separation range of the two channels (the IF frequency range) is determined by the properties of the IQ hybrid detectors (typically 1.5-10 GHz here). An additional U-band scalar horn, typically oriented to receive X-mode radiation, is used to detect the cross-polarization signal backscattered predominantly from the plasma cut-off locations. The signal paths for the backscattered CPS return signals are shown in green. The CPS signals for both launched frequencies are separated out via heterodyning, using two additional balanced mixers, with the LO input derived from the microwave source signals. After amplification (not shown here), IQ detectors with the same IF frequency range (typically

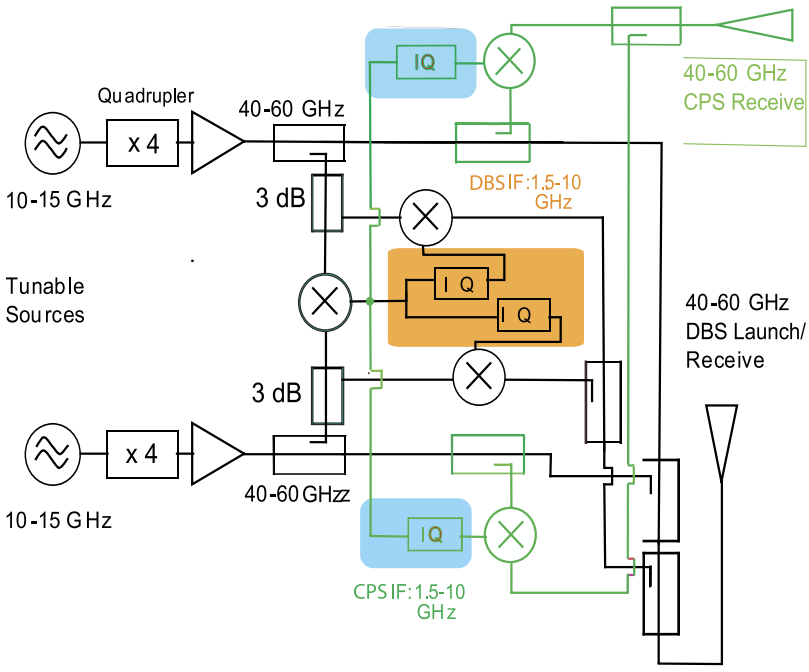

FIG. 5. Schematic of U-band microwave transceiver, including IF sections, for the combined DBS and CPS diagnostics. The U-band launch antenna (used also for monostatic DBS detection) and the horn used to detect the cross-polarized backscattered signal are also shown here. CPS signal paths are shown in green.

1.5-10 GHz) are used to detect the CPS signals (highlighted in blue here).

IV. GEOMETRY AND ALIGNMENT

For optimum spatial resolution, the DBS probing beam should be narrow and well focused on the plasma region of interest. Wavenumber resolution would however be improved with a larger diameter probing beam.[20,21] As described in more detail previously,[6,21] the wavenumber resolution of the backscattered signal depends, however, also on the toroidal and poloidal curvature of flux surfaces, and optimization for the expected C-2W plasma equilibria requires narrow probing beams with a Gaussian width of 3-6 cm. For these beam parameters and plasma curvature radii of 0.2-0.4 m in C-2W, a wavenumber resolution $\Delta k_\theta/k_\theta \leq 0.4$-$0.8$ is calculated. FRC plasmas in C-2W are also expected to slowly contract axially on a timescale of several ms, reducing their axial length in the confinement vessel. Since the DBS/CPS diagnostic will be installed close to but not exactly in the axial device midplane, a possible axial misalignment of the probing beam needs to be taken into account. Figure 6(a) shows trajectories of O-mode beams launched with different axial launch mismatch angles ϕ_L with respect to the magnetic field direction [as shown in Fig. 6(a)]; Fig. 6(b) shows the resulting local axial mismatch angles ϕ_0 of the launched microwave beam inside the plasma vs. radius, for different initial launch mismatch angles ϕ_L. To estimate the permissible beam misalignment, the change of the scattered power along the beam path can be expressed as[21]

$$\frac{dI}{dz} \propto \tilde{n}^2(k_n, z) \exp\left(-\frac{k_n^2 a_0^2 \sin^2(\phi_0)}{2}\right), \tag{4}$$

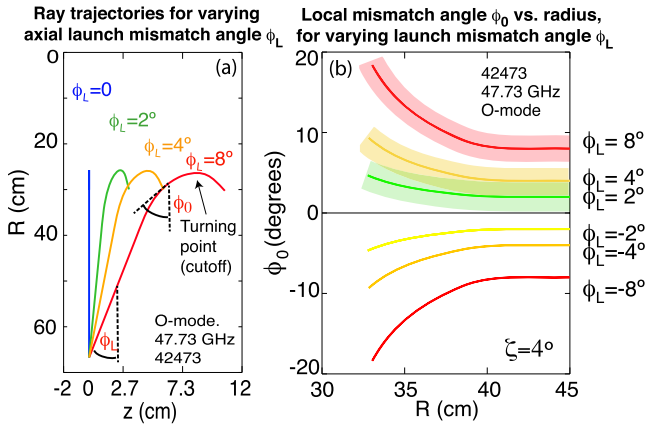

FIG. 6. (a) O-mode ray trajectory in a typical C-2U FRC plasma for different axial launch mismatch angles ϕ_L as indicated vs. radius R and coordinate z along the local magnetic field (referenced here to the launch point); (b) local O-mode mismatch angle ϕ_0 vs. radius in the plasma for different launch mismatch angles ϕ_L. ϕ_0 is increased substantially compared to ϕ_L due to beam refraction in the plasma [angles appear exaggerated in (a) due to expanded z-axis scale]. The toroidal launch angle (defined in Fig. 3) is $\zeta = 4°$.

where the index "n" denotes the density fluctuation wavenumber, a_0 is the beam radius, and ϕ_0 is the local axial mismatch angle at the turning point (cutoff), which is increased compared to the launch mismatch angle. Accordingly, significant scattered power is still received when the mismatch angle at the turning point satisfies $|\phi_0| \leq \sqrt{2/(2k_n a_0)}$, leading to permissible launch misalignment angles ϕ_L between ~8° and 1° for probed toroidal turbulence wavenumbers $k_\theta = 1$–$8\ \mathrm{cm}^{-1}$. Two-axis adjustability of the focusing mirror allows minimizing the axial beam misalignment, enabling useful data collection once the FRC has axially contracted, in addition to selecting the toroidal launch angle and hence the probed DBS and CPS wavenumber.

ACKNOWLEDGMENTS

We would like to acknowledge the support of the entire TAE team in the design and implementation of the DBS/CPS diagnostic.

[1] M. W. Binderbauer, T. Tajima, L. C. Steinhauer, E. Garate, M. Tuszewski, L. Schmitz, H. Y. Guo, A. Smirnov, H. Gota, D. Barnes *et al.*, Phys. Plasmas **22**, 056110 (2015).
[2] H. Gota, M. W. Binderbauer, T. Tajima, S. Putvinski, M. Tuszewski, E. Garate, S. Korepanov, A. Smirnov, M. C. Thompson, E. Trask, X. Yang, L. Schmitz, Z. Lin *et al.*, Nucl. Fusion **57**, 116021 (2017).
[3] J. C. Hillesheim, W. A. Peebles, T. L. Rhodes, L. Schmitz *et al.*, Rev. Sci. Instrum. **81**, 10D907 (2010).
[4] W. A. Peebles, T. L. Rhodes, J. C. Hillesheim, L. Zeng, and C. Wannberg, Rev. Sci. Instrum. **81**, 10D902 (2010).
[5] L. Schmitz, E. Ruskov, B. H. Deng, H. Gota *et al.*, Rev. Sci. Instrum. **85**, 11D840 (2014).
[6] L. Schmitz, D. Fulton, E. Ruskov, C. Lau, B. H. Deng *et al.*, Nat. Commun. **7**, 13860 (2016).
[7] D. P. Fulton, C. K. Lau, L. Schmitz, I. Holod, Z. Lin, M. W. Binderbauer, and TAE Team, Phys. Plasmas **23**, 056111 (2016).
[8] C. K. Lau, D. P. Fulton, I. Holod, Z. Lin, M. Binderbauer, T. Tajima, and L. Schmitz, Phys. Plasmas **24**, 116021 (2017).
[9] D. W. Ross, Plasma Phys. Controlled Fusion **34**, 137 (1992).
[10] W. Lee, J. R. Angus, and S. I. Krasheninnikov, Phys. Plasmas **22**, 072113 (2015).
[11] T. Lehner, D. Gresillon, X. L. Zou, and B. De Gentile, in *Proceedings of the 12th European Conference on Plasma Physics, Budapest*, edited by L. Pocs and A Montvai (EPS, Petit-Lancy, Switzerland, 1985), Vol. II, p. 644.
[12] T. Lehner, J. M. Rax, and X. L. Zou, Europhys Lett. **8**, 759 (1989).
[13] X. L. Zou, L. Laurent, and J. M. Rax, Plasma Phys. Controlled Fusion **33**(8), 903 (1991).
[14] L. Vahala, G. Vahala, and N. Bretz, Phys. Fluids B **4**, 619 (1992).
[15] X. L. Zou, L. Colas, M. Paume, J. M. Chareau *et al.*, Phys. Rev. Lett. **75**, 1090–1093 (1995).
[16] Y. Kogi, A. Mase, L. G. Bruskin, N. Oyama *et al.*, Rev. Sci. Instrum. **70**, 991–994 (1999).
[17] T. L. Rhodes, K. Barada, W. A. Peebles, and N. A. Crocker, Rev. Sci. Instrum. **87**, 11E726 (2016).
[18] N. Rostoker and A. Querushi, Phys. Plasmas **9**, 3057 (2002).
[19] A. P. Smirnov and R. W. Harvey, "The GENRAY ray tracing code," CompX Report COMPX-2000-01, 2001.
[20] E. Blanco, T. Estrada, and J. Sanchez, Plasma Phys. Controlled Fusion **48**, 699 (2006).
[21] J. C. Hillesheim, N. A. Crocker, W. A. Peebles, H. Meyer *et al.*, Nucl. Fusion **55**, 073024 (2015).